PERGAMON

International Journal of Solids and Structures 37 (2000) 5773–5794

INTERNATIONAL JOURNAL OF SOLIDS and STRUCTURES

www.elsevier.com/locate/ijsolstr

Mechanical behavior of a syntactic foam: experiments and modeling

Egidio Rizzi[a], Enrico Papa[b], Alberto Corigliano[b,*]

[a]*Politecnico di Bari, Facoltà di Ingegneria di Taranto, Dipartimento di Ingegneria Strutturale, via Orabona 4, I-70125 Bari, Italy*
[b]*Politecnico di Milano, Dipartimento di Ingegneria Strutturale, piazza Leonardo da Vinci 32, I-20133 Milano, Italy*

Received 20 May 1999; in revised form 27 July 1999

Abstract

This paper reports the results of a research activity concerning the mechanical behavior of a syntactic foam employed as core material for sandwich composite panels. Following a purely phenomenological approach, experimental and numerical results are presented and compared at the macroscopic scale. The main features observed in the uniaxial, biaxial and Three Point Bending (TPB) tests are highlighted. A bimodulus constitutive model of the Drucker–Prager type is chosen for modeling biaxial stress states with diffused damage. An alternative discrete crack approach is devised for the computer simulation of the (TPB) three point bending tests: the best matching is achieved for a rectangular Dugdale-type cohesive law. Though not proposing novel experimental or numerical methodologies, the present engineering approach should interest readers generally involved in computational composite mechanics and, specifically, in modeling particulate composites of the type considered here. © 2000 Elsevier Science Ltd. All rights reserved.

Keywords: Composites; Syntactic foams; Experiments; Uniaxial tension/compression; Biaxial compression; Three point bending; Constitutive models; Cohesive laws; Finite element simulations

1. Introduction

The present paper reports the results of a research study on the mechanical behavior of a syntactic foam made with an epoxy resin matrix embedding randomly dispersed hollow glass microspheres. Among other uses, this syntactic foam can be employed as a light core material for composite sandwich panels with woven glass fiber skins to be used in naval engineering.

After a short review on general definitions and properties of the particulate composite materials,

* Corresponding author. Tel.: +390-2-2399-42-44; fax: +390-2-2399-42-20.
E-mail address: coriglia@stru.polimi.it (A. Corigliano).

0020-7683/00/$ - see front matter © 2000 Elsevier Science Ltd. All rights reserved.
PII: S0020-7683(99)00264-4

usually called syntactic foams, the paper focuses on the syntactic foam under study. The salient features of the mechanical behavior observed under uniaxial tension/compression, biaxial compression and Three Point Bending (TPB) experimental tests are summarized first. The material is rather ductile in compression, extremely brittle in tension, and displays different elastic stiffnesses (bimodulus material). The biaxial failure domain has an egg-shaped form, typical of particulate composite frictional materials such as concrete. The response under TPB is rather brittle for the specimen size chosen but allowed an indirect estimation of the Mode-I fracture energy.

Modeling is then considered. Finite Element (FE) simulations are performed with the commercial computer code ABAQUS (Hibbitt et al., 1998). A Modified Drucker–Prager model is calibrated on the basis of the experimental biaxial failure points. The model is complemented by a procedure devised to account for the different material stiffnesses in tension and compression. A computational technique based on local stiffness release is also implemented to capture the brittle response under tension. The model performs well in preliminary FE simulations of the homogeneous uniaxial/biaxial tests. However, in the FE analyses of the TPB test, which clearly involve brittle fracture of the notched specimens, qualitative-only agreement with the experimental results is achieved: peak load is considerably underestimated. Then, an alternative discrete crack approach is considered by placing a cohesive crack law on the ligament section at mid-span. Different shapes of the cohesive law are tested: the rectangular Dugdale-type cohesive law provides the best quantitative comparison with the experimental data.

2. Syntactic foams

2.1. Generalities

A comprehensive and detailed survey on syntactic foams and related literature is provided by Shutov (1986), where a list of 194 references is available. This section provides just a brief introduction and overview for the ease of the reader. Syntactic foams are a special kind of particulate composite materials made by a matrix (“*binder*”) and a gas-filled aggregate (“*filler*”) consisting of hollow spherical microspheres (Luxmoore and Owen, 1982). These composite materials are classified as foams since they possess a structure formally similar to that of a cellular, gas-expanded, solidified liquid. The term syntactic (from the Greek “*syntaktikós*” — orderly disposed system) indicates a constructed foam, in the sense that the material is manufactured by a specific mixing procedure of fillers and binders with appropriate volume fractions. However, the filler is randomly dispersed in the matrix, in a way to obtain an homogeneous and isotropic macroscopic behavior.

Syntactic foams are normally tertiary systems, since matrix and gas-filled aggregate are usually made of different materials: thermosetting polymers such as epoxy and phenolic resins, polyimides, polyurethanes and silicons are often used as binders; glass, carbon, metal, and resin made of microbubbles are frequently taken as fillers. However, syntactic foams are basically classified as two-phase systems, when they do not contain dispersed air bubbles between binder and filler (vacuum manufacturing), or as three-phase systems, when air bubbles are included, in some cases on purpose, in view of lowering the foam density (Puterman et al., 1980; Narkis et al., 1980).

2.1.1. Properties and applications

Thermosetting polymers as opposed to thermoplastic polymers are normally preferred binders due to easier manufacturing technologies (Puterman et al., 1980; Parodi, 1989; Hollaway, 1990) rather than better specific material properties (Hull and Clyne, 1996). The properties of the resulting syntactic foam, especially mechanical ones, are more directly tied to filler type and filler/binder interaction. Normally, the preferred filler geometry is spherical, which allows the best packing factor and hydrostatic

compression strength. Sphere diameters usually range from 1 μm to 100 mm. Frequently used bubbles, referred to as microspheres, have a diameter in the range 1–500 μm and wall thickness of 1–4 μm. Macrospheres of diameter larger than 500 μm are more seldomly used (Shutov, 1986). Glass microbubbles are frequently preferred due to mechanical strength, smoothness and regularity of the surface, good wetting characteristics and low viscosity of the resulting foam, all this combined with well-established production procedures and low cost.

Low degree of water absorption is one of the peculiar properties of syntactic foams; it mainly depends on the chemical and physical properties of filler and binder and their volume ratio. Thermal properties are normally dominated by the matrix characteristics; among polymers, polyimides show the best mechanical properties at increasing temperature. Syntactic foams are also characterized by good thermal insulation and dielectric properties (Shutov, 1986). Concerning the mechanical behavior, syntactic foams display at best uniaxial compression strengths of about 100 MPa, hydrostatic compression strengths around 150 MPa, uniaxial tension strengths of about 25–30 MPa, tensile Young's modulus around 2500–3000 MPa. The behavior in compression is quite ductile, whereas tensile response is rather brittle (Luxmoore and Owen, 1982). DeRuntz and Hoffman (1969) reported an experimental investigation on an epoxy matrix/hollow glass microspheres foam with low degree of dispersed air bubbles, tested under biaxial and triaxial stress states: the failure locus is closed in the principal stress space so that the material exhibits a finite strength under triaxial compression. The hydrostatic pressure/volumetric strain diagram takes a typical sigmoidal form, with a central part at almost constant pressure which corresponds to progressive sphere crushing (Luxmoore and Owen, 1982). Other experimental investigations on the mechanical behavior of syntactic foams are available in the literature; most of them are devoted to the determination of Young's moduli and uniaxial tension and compression strengths, often seen as a function of the weight fractions of the constituents; the experimental results are frequently compared to predictions based on analytical and FE micromechanical computations (Sahu and Broutman, 1972; Nicolais and Nicodemo, 1973; Okuno and Woodhams, 1974; Narkis et al., 1980; Nielsen, 1983; Wei et al., 1989; Palumbo et al., 1996). The modelizations at the macroscopic level are rather scant (DeRuntz and Hoffman, 1969; DeRuntz, 1971).

The spectrum of engineering applications of syntactic foams is quite broad. First and more significant applications of syntactic foams date back to the 50 in the area of naval and marine engineering (see Luxmoore and Owen, 1982; Shutov, 1986; Smith, 1990), where they have been used for structural elements such as hulls, ribs and decks (Palchak, 1973), for components at deep depth (up to 12,000 m) such as submarines, submerged buoys, deep sea platforms and pipe joints, and for shielding and repairing submerged apparatuses (Lee and Neville, 1973; Sternfield, 1982). Syntactic foams are often used in civil and industrial engineering, in construction and as an imitation of wood and marble (Shutov, 1986); often they are employed as core materials due to good shear stiffness and strength, fatigue and impact resistance (Hiel et al., 1993; Scarponi et al., 1996). Syntactic foams made with glass and more often carbon microbubbles are widely used in aeronautical and aerospace engineering as fillers of alveolate structures (Lee and Neville, 1973) and as protection shields for space vehicles and missile heads (Thomas, 1973). In motorcar industry, syntactic foams have been used for spoilers, dashboards and roofs (Sternfield, 1982). They are also employed in electronics and telecommunication fields for shielding electronic components or cables from vibrations, electromagnetic fields, radiations and high temperatures (Mildner et al., 1970; Puterman et al., 1980; Sternfield, 1982).

2.2. The syntactic foam under study

The syntactic foam under study was manufactured by a former house of Intermarine SpA under the trademark Tencara 2000™. The foam is made by an epoxy resin matrix binding hollow air-filled glass microspheres. The matrix is made with SP Ampreg 20™ epoxy resin treated with SP Ampreg™

Table 1
Tensile mechanical properties of epoxy resin SP Ampreg 20™ treated with SP Ampreg™ UltraSlow hardener (manufacturer data — SP systems

Cure scheme	Tensile strength (MPa)	Elongation to break (%)	Tensile modulus (MPa)
5 h at 80°C	71	> 5.0	3200
16 h at 50°C	77	4.0	3300
4 weeks at room temperature	57	2.5	3400

UltraSlow hardener. Table 1 reports the data provided by the manufacturer on the salient mechanical features of the epoxy matrix for different curing schemes. Air-filled hollow glass microspheres named 3M Scotchlite™ Glass Bubbles, type K1, are made with a water resistant, chemically stable, borosilicate glass. Bubbles have an average diameter of 70 μm and wall thickness of 0.58 μm. Table 2 reports some of the microbubbles data as given by the manufacturer. At eye-sight, the filler appears as a fine white powder.

The syntactic foam is prepared by mixing resin and hardener under vacuum and by adding microspheres until full homogenization; weight ratios are: 300 for resin, 100 for hardener, and 54 for microspheres. Polymerization lasts initially for 24 h at room temperature and eventually for 16 h at 50°C. There is no special treatment of glass surfaces or introduction of bonding agents (e.g. silanes); such procedures are known to improve strength significantly (Kenyon, 1968; Palumbo et al., 1996). The syntactic foam is quite similar to a foam previously studied at the University of Brescia: a detailed description of the manufacturing process of that foam is given in Palumbo et al. (1996). Fig. 1 displays a SEM image of the present syntactic foam, which displays an average measured density of 0.55 g/cm^3.

3. Experimental results

This section reports the experimental results on the mechanical behavior of the Tencara 2000™ syntactic foam specimens. The tests were performed at the Department of Structural Engineering, Politecnico di Milano. The complete set of experimental data, including the investigation on the composite sandwich whose core is made with the syntactic foam, are given separately (Papa et al., 1999). Here, the main results of the following uniaxial tension/compression, biaxial compression and TPB tests are presented:

- three uniaxial compression tests under displacement control on cylindrical specimens;

Table 2
Properties of Scotchlite™ Glass Bubbles type K1 (manufacturer data — 3M Italia)

Density (ASTM D2840, 1984 edition)	0.125 g/cm^3
Apparent density	0.075 g/cm^3
Average wall thickness	0.58 μm
Average diameter	70 μm
Residual on 177 μm sieve (ASTM D1214)	5% in weight
Survival at 1.7 MPa hydrostatic pressure (TM-2028)	80%
Oil absorption (ASTM D1483)	31–36 g of oil per 100 cm^3 of spheres
Thermal conductivity at 21°C	0.03–0.17 W/m K
Dielectric constant	1.15
Refractive index	1.07

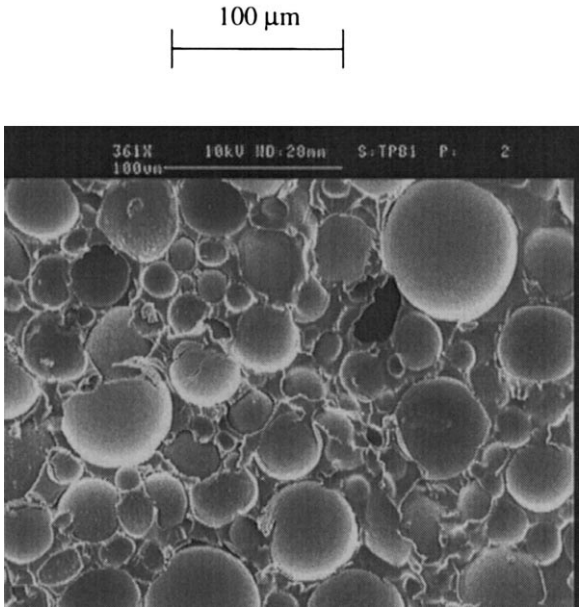

Fig. 1. Scanning Electron Microscopy (SEM) of syntactic foam Tencara 2000℠ (courtesy of M. Palumbo and E. Tempesti, Università di Brescia).

- three uniaxial tension tests under displacement control on axisymmetric specimens with tapered cross-sections;
- five biaxial compression tests under force control on squared panels along radial paths with different biaxial stress ratios;
- four TPB tests under deflection control on prismatic specimens with rectangular cross-section and preformed notch at mid-span.

Specimen dimensions have been chosen according to UNI and ASTM standards, to the characteristics of the loading devices and on the basis of some preliminary tests on a similar syntactic foam (Palumbo et al., 1996), which, however, displayed better mechanical performances. Specimens were prepared directly by the manufacturer. Strains were measured by electric strain gauges directly glued onto the specimens.

3.1. Uniaxial tension/compression tests

Uniaxial tests have been performed on a MTS 329.10 S machine. The actuator has a bearing capacity of $\pm$100 kN, with maximum stroke of 150 mm. It incorporates a Linear Variable Differential Transducer (LVDT); the loading cell is mounted on the bottom of the loading frame. Displacement has been imposed from top at a rate of 0.5 mm/min.

For the compression tests, specimen shape and size were determined according to UNI 6132-72 standard for concrete and to ASTM D 695 M-91 standard for composites. Fig. 2 depicts the cylindrical specimen geometry and a sketch of the test scheme. Two teflon sheets were interposed between specimen and loading platens to reduce friction. Guideline for tensile specimens geometry was the ASTM D 638 standard for composite materials. It recommends flat "*dog bone*"-shaped specimens with appropriate ranges of relative dimensions. Due to ease of workability by the manufacturer, axisymmetric bars with

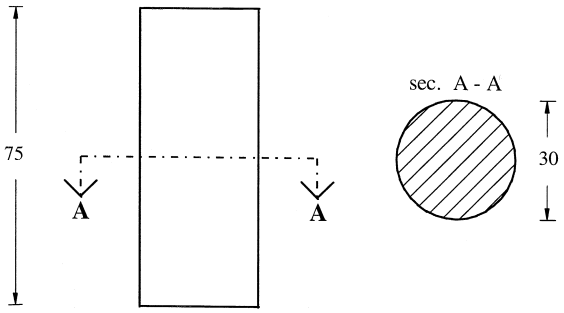

(a)

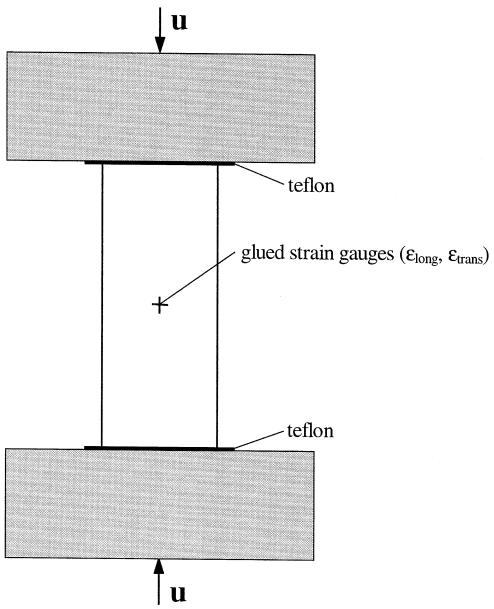

(b)

Fig. 2. Uniaxial compression tests of syntactic foam Tencara 2000™: (a) specimen geometry; (b) test scheme (displacement control). Dimensions in mm.

Table 3
Mechanical properties of syntactic foam Tencara 2000™: uniaxial tension tests

Young modulus, E_c	1600 MPa
Poisson ratio, ν	0.34
Compressive strength, f_c	28.39 MPa
Peak strain, ε_{cpeak}	2.25%

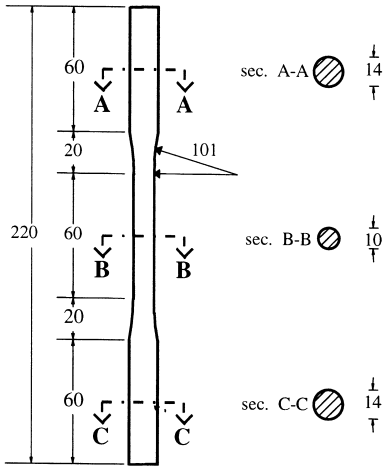

(a)

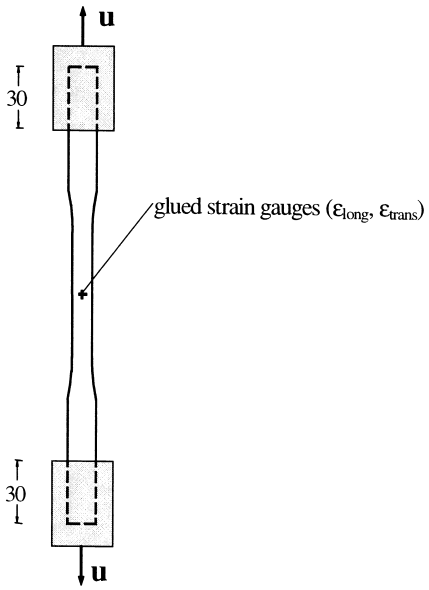

(b)

Fig. 3. Uniaxial tension tests of syntactic foam Tencara 2000®: (a) specimen geometry; (b) test scheme (displacement control). Dimensions in mm.

tapered cross-sections have been preferred. Fig. 3 displays specimen geometry and scheme of the tensile test.

The stress/strain curves of the uniaxial tests are reported in Fig. 4. Tables 3 and 4 give the average mechanical properties in compression and tension. Tensile strength $f_t = 15.63$ MPa is about 55% of the

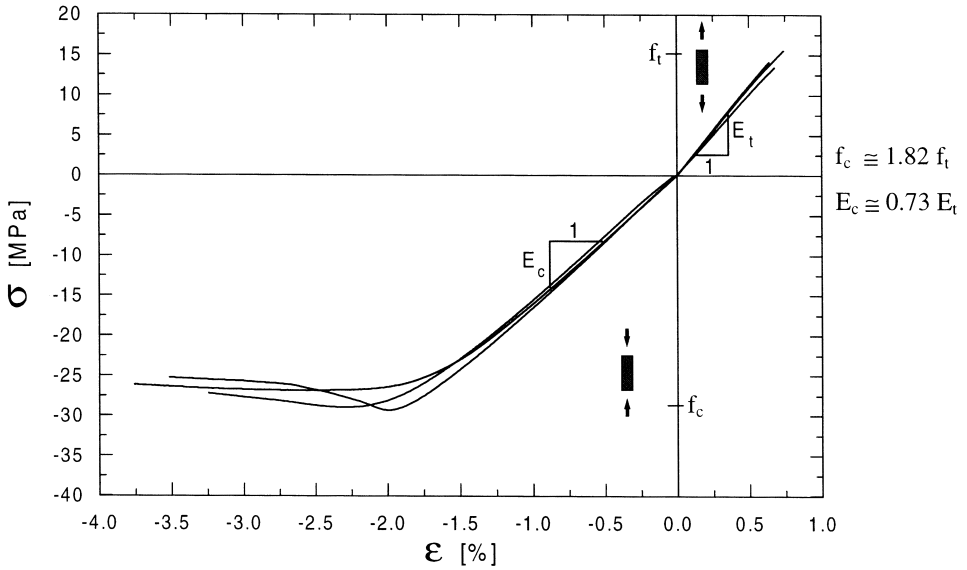

Fig. 4. Uniaxial nominal stress/strain curves of syntactic foam Tencara 2000™ in tension and compression (traction positive).

compressive strength $f_c = 28.39$ MPa. The observed responses are in qualitative agreement with the behavior normally displayed by syntactic foams with glass microspheres (Luxmoore and Owen, 1982).

Compression behavior is rather ductile, with a softening post-peak branch which tends to stabilize on an horizontal plateau at residual strength. Loading/unloading paths performed in some of the compression tests showed that elastic stiffness degradation is not particularly significant (Papa et al., 1999). The collapse mechanism is due to strain localization along a shear band inclined to an angle of about 45° with respect to the loading axis. The band separates the specimen into two parts that glide with respect to each other: interlocking and friction govern the behavior after the onset of strain localization and may explain the residual strength observed for the nominal stress/strain curves.

The response under tension is instead perfectly brittle with rupture on a section perpendicular to the loading axis. The tensile peak coordinates reported in Table 4 were taken from the only test which displayed fracture in the central part of the specimen; the other two tests registered breakage in zones near the tapered sections and showed slightly lower tensile strengths (Fig. 4).

The tests showed different elastic stiffnesses in tension and compression (bimodulus material): Young's modulus in tension $E_t = 2200$ MPa is about 35% greater than that in compression $E_c = 1600$ MPa. This phenomenological feature is not normally reported in the literature on syntactic foams. First of all, part of the difference should be attributed to the fact that the specimens tested in tension belonged to a second set of syntactic foam specimens which displayed lower degree of porosity and about 15% higher compressive stiffness (~1850 MPa). The remaining 20% difference should be mainly attributed to the

Table 4
Mechanical properties of syntactic foam Tencara 2000™: uniaxial compression tests

Young modulus, E_t	2200 MPa
Poisson ratio, ν	0.34
Tensile strength, f_t	15.63 MPa
Peak strain, ε_{tpeak}	0.75%

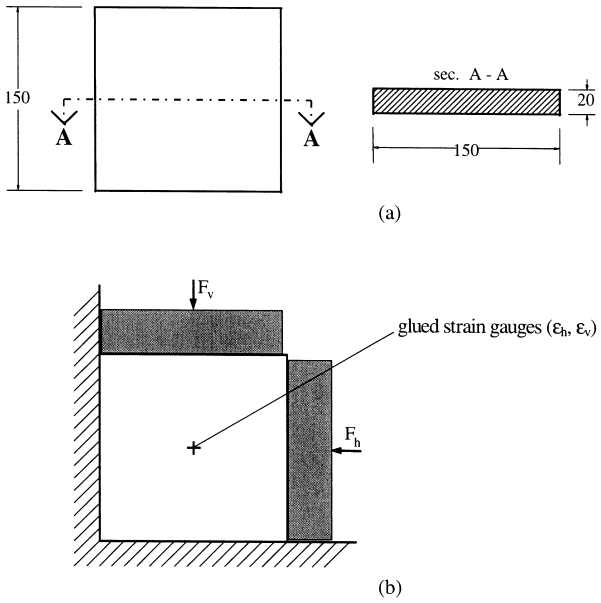

Fig. 5. Biaxial tests of syntactic foam Tencara 2000™: (a) specimen geometry; (b) test scheme (force control: radial paths F_h, F_v). Dimensions in mm.

presence of air bubbles between matrix and filler. Also, sphere wall thickness seems to play a crucial role under compression (Nielsen, 1983): other compression tests performed on a foam made with same glass bubbles but with about twice the wall thickness (bubbles type K37; average diameter 50 μm and wall thickness 1.28 μm), showed considerable increase of stiffness (Papa et al., 1999). Poisson's ratio was rather unaffected by the sign of the applied stress: the average value of $\nu = 0.34$ was recorded.

The shear modulus of about $G = 780$ MPa, which was measured on torsion tests on specimens of the same type as those of the tensile tests, is quite in agreement with a shear modulus evaluated with the classical formula for isotropic linear elastic materials where the tensile modulus is taken as Young's modulus and Poisson's ratio is equal to 0.34. This seems to support the conjecture that the tensile modulus would be the intrinsic elastic stiffness of a syntactic foam without unintentionally included voids. Hypothesis of isotropy seems consistent for that case.

Table 5
Mechanical properties of syntactic foam Tencara 2000™: biaxial compression tests

Horizontal/vertical load ratio, F_h/F_v	Horizontal peak stress, σ_h (MPa)	Vertical peak stress, σ_v (MPa)
0/1	0.00	−27.60
1/3	−11.70	−35.12
2/3	−21.57	−36.90
1/1	−31.33	−31.33
1/1	−30.41	−30.41

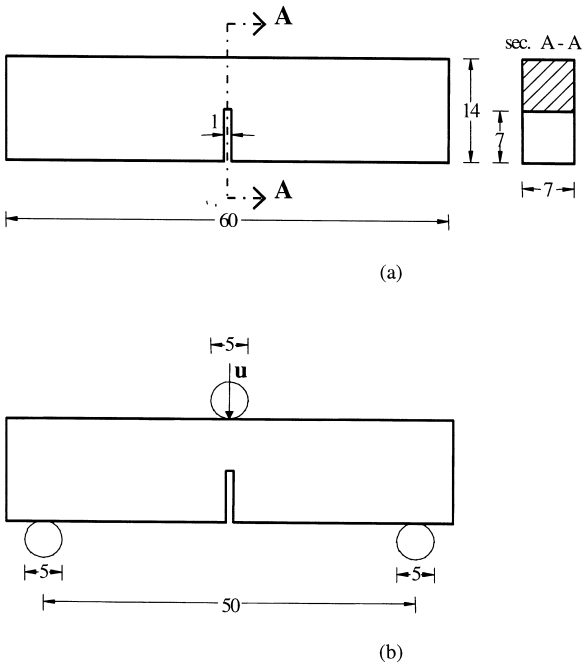

Fig. 6. Three Point Bending (TPB) tests of syntactic foam Tencara 2000™: (a) specimen geometry; (b) test scheme (displacement control). Dimensions in mm.

3.2. Biaxial compression tests

Biaxial compression tests were made on a biaxial fatigue testing device equipped with two actuators: the horizontal one has a maximum load capacity of 100 kN, the vertical one features a maximum load of 300 kN. Both actuators incorporate a loading cell and an LVDT. Allowable frequency range of cyclic tests is 0.1–30 Hz. Each actuator has a maximum stroke of $\pm$25 mm.

Tests were made on squared panels under force control (Fig. 5); three different radial paths in compression/compression with horizontal to vertical force ratios of 1/3, 2/3, 1/1 were imposed. Loading rate was 30 kN/min. A uniaxial compression test 0/1 was also performed for comparison with the compression tests on cylindrical specimens: the compressive strength obtained was about the same. Table 5 reports the failure points corresponding to peak load: they suggest a failure locus with an egg-shaped form (Fig. 7) similar to biaxial failure domains of frictional geomaterials. Failure has been always characterized by microsphere crushing on an horizontal layer near the upper vertical platen.

3.3. Three point bending (TPB) tests

TPB tests on notched specimens were made on an Instron 8652 loading machine with bearing capacity of 100 kN and frequencies between 0 and 1 Hz. A servocontrolled electromechanical actuator with LVDT incorporated imposes the displacement from bottom; the loading cell is mounted on top of the loading frame.

Specimen dimensions have been chosen according to the ASTM E 399 standard as a compromise between optimum size for the testing machine and small enough size to avoid too brittle response (Fig. 6). Such size was estimated on the basis of previous tests on a similar foam, which however turned

out to present higher fracture toughness. Due to the small specimen dimensions, it was impossible to drive the test under crack mouth opening; thus the tests were made under vertical displacement control at a rate of 0.2 μm/s.

The four load/vertical displacement curves are shaded in Figs. 9–12. The observed responses are quasi-brittle: after peak, there is a sudden, almost vertical, load drop, which seems to suggest a possible snap-back path if the feed-back control on crack opening would have been used. A softening tail develops after the sudden drop. All specimens collapsed by fracture at mid-span section, which departed and propagated vertically from right above the sharp-edged notch.

4. Modeling and calibration of material parameters

The experimental investigation showed qualitative features typical of frictional pressure-dependent geomaterials with different behaviors in tension/compression. Two models are selected pertaining, respectively, to the smeared approach of continuum mechanics and to the discrete crack approach of fracture mechanics: a Modified Drucker–Prager elastoplastic model and a cohesive crack model. Both are calibrated on the basis of the experimental tests and are separately used for the numerical simulations presented in Section 5.

4.1. Modified Drucker–Prager elastoplastic model

Within the smeared approach of continuum mechanics, among other constitutive models, elastoplastic model of Drucker–Prager type seems to be an appropriate choice for modeling the syntactic foam under biaxial stress states. A Modified Drucker–Prager model of this type is available in the FE code employed for the numerical analyses.

The yield function f is defined in terms of two parameters (K and φ) which introduce a dependence on the hydrostatic stress (first invariant of the stress tensor, $I_1 = \mathrm{tr}\,\boldsymbol{\sigma}$) and on the second and third invariants of the stress deviator $\mathbf{s}$ (J_2, J_3):

$$f = t + p\tan\varphi - b(\epsilon_p), \quad \text{with } t = \frac{1}{2}q\left[1 + \frac{1}{K} - \left(1 - \frac{1}{K}\right)\left(\frac{r}{q}\right)^3\right], \tag{1}$$

where the stress invariants p, q and r are defined as

$$p = \frac{I_1}{3} = \frac{\sigma_{ii}}{3}, \quad q = \sqrt{3J_2} = \sqrt{\frac{3}{2}s_{ij}s_{ij}}, \quad r = \sqrt[3]{\frac{27}{2}J_3} = \sqrt[3]{\frac{9}{2}s_{ij}s_{jk}s_{ki}} \tag{2}$$

(summation convention is used). In Eq. (1), $b(\epsilon_p)$ is the isotropic hardening function and ϵ_p is an internal variable which accounts for the plastic strain history (strain-hardening). Function $b(\epsilon_p)$ is assigned at input stage in terms of the uniaxial stress/plastic strain curve in compression. Parameter φ controls the opening of the cone-shaped yield surface in principal stress space, while K governs the J_3-dependence. The classical Drucker–Prager model is obtained for $K = 1$ (which implies $t = q$), while the von Mises model is obtained for $K = 1$ and $\varphi = 0$. The yield surface is convex for values of K between 7/9 and 1 (Hibbitt et al., 1998) and is opened in the meridian plane. This contrasts the already-mentioned experimental observations by DeRuntz and Hoffman (1969): under triaxial compression, the model should then be completed by an appropriate cap. For simplicity, and due to lack of experimental data, plastic flow is assumed associative.

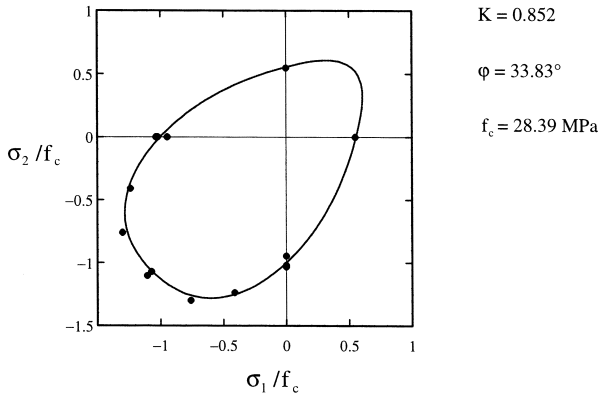

Fig. 7. Experimental failure points of syntactic foam Tencara 2000™ under biaxial stress and calibrated Modified Drucker–Prager failure domain.

4.1.1. Calibration of the elastoplastic model

To characterize the failure domain in the biaxial stress plane (σ_1, σ_2), it is imposed that the yield surface at peak stress contains the point $(-f_c, 0)$, with the average value $f_c = 28.39$ MPa as recorded from the uniaxial compression tests. From Eq. (1), for $f = 0$, in uniaxial compression b is given as

$$b = \left(1 - \frac{1}{3}\tan\varphi\right) f_c. \tag{3}$$

Once b is fixed, the failure surface depends only on the two parameters K and φ.

A first identification procedure of K and φ may be based on three characteristic strength values. In our case, f_t, f_c and f_{bc}, namely tension, compression and equi-biaxial compression strengths, respectively, are available. From Eqs. (1)–(3), K and φ can then be expressed as:

$$K = \frac{f_c f_{bc} - f_c f_t + 3 f_t f_{bc}}{f_c(f_t + 2 f_{bc})}, \qquad \tan\varphi = 3\frac{f_c - (f_t/K)}{f_c + f_t}. \tag{4}$$

Taking $f_t = 15.63$ MPa and $f_c = 28.39$ MPa from the uniaxial tests and choosing the average value $f_{bc} = 30.87$ MPa of the two equi-biaxial compression readings 30.41 and 31.33 MPa (Table 5), Eq. (4) renders

$$K = 0.856, \quad \varphi = \arctan(0.6904) = 34.62^\circ. \tag{5}$$

A second, more accurate, calibration procedure can take advantage of the available failure points under biaxial compression (last four rows of Table 5) and uniaxial tension. By using a linear least square approximation (Bard, 1974), the following estimates are obtained:

$$K = 0.852, \quad \varphi = \arctan(0.6701) = 33.83^\circ. \tag{6}$$

Values (5) and (6) of K and φ are quite close to each other. For the numerical computations, estimates (6) have been adopted; the relevant biaxial failure domain is plotted in Fig. 7.

Once the failure surface is known, it is possible to locate failure points along untested radial paths. In particular, for the equi-biaxial tensile strength f_{bt}, one gets

$$f_{bt} = \frac{f_c f_t f_{bc}}{f_c f_{bc} - f_c f_t + f_t f_{bc}} = \frac{3 - \tan\varphi}{3 + 2\tan\varphi} f_c. \tag{7}$$

With calibration (5), $f_{bt} = 14.97$ MPa, whereas for the adopted values (6), $f_{bt} = 15.23$ MPa. The equi-biaxial tensile strength provided by the model is thus slightly lower than the uniaxial tensile strength $f_t = 15.63$ MPa.

4.2. Cohesive crack model

Within the discrete crack approach of fracture mechanics, the cohesive crack model describes the material behavior in the "*process zone*" or "*craze*" right in front of the crack tip (Dugdale, 1960; Barenblatt, 1962; Hillerborg et al., 1976; Cen and Maier, 1992; Maier et al., 1993). Such process zone accounts for the dissipative processes due to fracturing while the bulk material is assumed linearly elastic. In the present study, only pure Mode-I fracture processes are considered: the cohesive law is then expressed by a σ_n/w law, where σ_n is the component of stress normal to the fracture and w is the crack opening displacement in the same normal direction. The area underneath the σ_n/w curve represents the fracture energy G_f, namely the energy per unit area dissipated during the fracture process.

Different cohesive crack laws have been proposed, ranging from linear to bilinear with break point and concave shape, and to parabolic or exponential. Various techniques have been suggested for the identification of the material parameters of such models (RILEM, 1985; Cornelissen et al., 1986; Karihaloo, 1995). The initial shape of the σ_n/w law may influence considerably the bearing capacity of concrete beams (Alvaredo and Torrent, 1987; Guinea et al., 1997); the tail of the softening law affects rather the post-peak response. In the present case, the linear and trapezoidal laws displayed in Figs. 11a and 12a are considered. Such choice is due to the limited experimental results which allow estimation only of f_t and G_f. The trapezoidal law is conceived in view of a parametric study. Its convex shape, rather than the typical concave bilinear shape often used for concrete materials, turned out to give the best quantitative results for the simulation of the TPB tests.

The classical linear law (Hillerborg et al., 1976) is characterized by two parameters only: the ultimate tensile stress σ_{n_u} and the critical opening displacement w_c after which the material is not able to carry further stress (Fig. 11a). The trapezoidal law is identified also by a third parameter $0 \leq \beta \leq 1$ which defines the position of the corner on the vertical edge of the cohesive law at $w = w_c$ (Fig. 12a). The two extreme values $\beta = 0$ and 1 correspond to the above-mentioned linear law and to the rectangular Dugdale-type cohesive law (Dugdale, 1960), respectively. The critical opening displacement w_c is normally expressed in terms of fracture energy G_f and ultimate tensile stress σ_{n_u}. For the trapezoidal law, the following relation applies:

$$w_c = \frac{2G_f}{(1+\beta)\sigma_{n_u}}. \tag{8}$$

4.2.1. Calibration of the cohesive crack model

The parameters of the cohesive law have been identified in terms of the experimental results of the uniaxial and TPB tests. The ultimate tensile stress has been taken equal to the uniaxial strength: $\sigma_{n_u} = f_t = 15.63$ MPa. The fracture energy G_f has been estimated as the average of the areas underneath the four load/vertical displacement (F/u) curves of the TPB tests:

$$G_f = \frac{\sum_{i=1}^{4}\left(\int_0^\infty F_i(u)\,du\right)/4}{A_{ligament}} \simeq 0.320 \text{ N/mm}, \tag{9}$$

where $A_{ligament} = 7 \times 7$ mm^2 is the nominal ligament section at mid-span (Fig. 6). With the above

values of σ_{n_u} and G_f, the critical opening displacement w_c, Eq. (8), ranges from 0.020 mm for $\beta = 1$ to 0.040 mm for $\beta = 0$. More appropriate identification procedures should account for factors affecting the loading readings, such as specimen and loading device masses (RILEM, 1985), and for the amount of plastic dissipation involved in the bulk material (Bažant, 1996).

5. Numerical FE simulations

The computational procedures which complemented the material models for the computer simulations of the experimental tests are now presented. The implementation has been checked on the homogeneous tests. Here, the FE results of the TPB test are given, with direct comparison to the experimental data. The best matching is obtained with the discrete crack approach based on the Dugdale-type cohesive crack law.

5.1. Computational techniques

To account for the different behaviors in tension and compression, the material models presented in Section 4 have been complemented by the two simple computational techniques described below. The cohesive crack law has been implemented through the use of nonlinear spring elements acting on the nodes of the ligament section at mid-span of the TPB specimen.

5.1.1. Bimodulus material

To include the different elastic stiffnesses in tension and compression, a simple criterion for discriminating between tension and compression stress states is conceived, which is based on the sign of the first stress invariant. The criterion has been implemented through a user subroutine; the Young's modulus E is defined as a field variable in the Gauss Points:

$$\begin{aligned} &\text{if} \quad \operatorname{tr}\boldsymbol{\sigma} \geq 0, \quad E = E_t; \\ &\text{if} \quad \operatorname{tr}\boldsymbol{\sigma} < 0, \quad E = E_c, \end{aligned} \tag{10}$$

where E_t and E_c are the Young's moduli in tension and compression, respectively. Poisson's ratio is constant. This criterion is supported by theoretical considerations on continuous piecewise-linear hyperelastic laws of isotropic materials (Curnier et al., 1995). Indeed, consistently with such derivations, the shear moduli of an isotropic material should be the same in the tension and compression subdomains, which would imply different Poisson's ratios. This would mean that the presence of voids, which could explain the bimodularity (Section 3.1), should also induce loss of macroisotropy. However, this aspect has not been taken into account in the present analyses.

5.1.2. Local stiffness release

To induce the brittle response under tension states, a simple computational technique of local stiffness release at Gauss Point level has been attempted. The procedure is implemented through a user subroutine: when a threshold value of a certain scalar failure index is reached in the single Gauss Point, the tensile elastic modulus E_t is annihilated locally. Such simple procedure seems easier and cheaper than alternative, more elaborated techniques, such as progressive element removal with remeshing. Different failure indexes may be considered, either based on local strain or stress states. As expected, strain indicators turned out to induce strongly mesh-dependent responses; on the other hand, apparently, stress indexes gave rise to rather mesh-insensitive results. As probably the most natural choice in brittle fracture, the local stiffness release was based on the value of the maximum principal

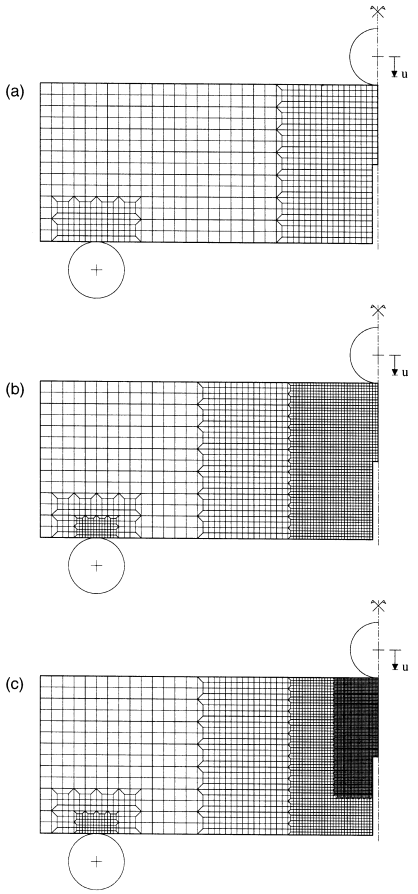

Fig. 8. Finite Element discretizations of TPB tests (displacement control). Quadrilateral four-noded isoparametric elements: (a) coarse mesh – 852 FE; (b) fine mesh – 2502 FE; (c) minute mesh – 4405 FE.

stress σ_1. The stiffness release criterion may then be expressed as:

$$\text{if } \sigma_1 \geq \sigma_1^{\text{cr}} = \alpha f_t, \quad E_t = 0, \tag{11}$$

where parameter α brings in a relation between the local threshold value and the material tensile strength f_t. Though the most natural choice would appear $\alpha = 1$, it is not said that this option renders the best results in terms of load bearing capacity and energy dissipation. A parametric study on different values of α is given in Section 5.2.1 for the TPB test.

5.2. Simulations of the TPB test

All analyses are quasi-static and based on the assumptions of plane stress and small displacements. Fig. 8 displays the three adopted discretizations of quadrilateral four-noded isoparametric elements. Supports and die are modeled by rigid rollers. Loading is imposed by the vertical displacement of the die.

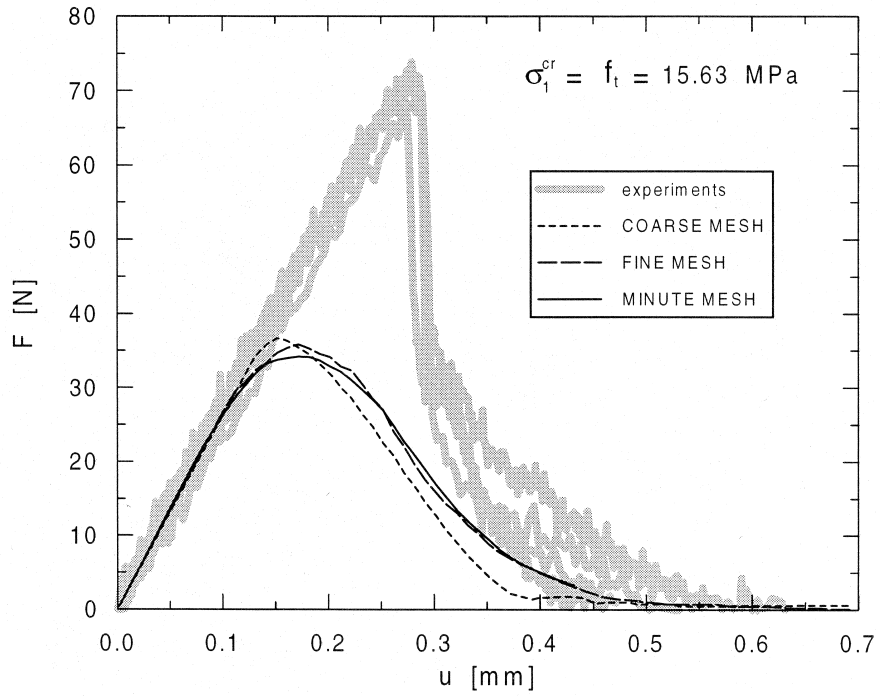

Fig. 9. Load/displacement curves of syntactic foam Tencara 2000℠ TPB test: Modified Drucker–Prager model with use of stiffness release technique based on critical value of the maximum principal stress σ_1 equal to tensile strength ($\sigma_1^{cr} = f_t$); comparison of the three meshes shows reduced mesh sensitivity; peak load is considerably underestimated.

5.2.1. Smeared crack approach

The Modified Drucker–Prager model is used in conjunction with the two techniques implemented to account for bimodularity and local stiffness release. The uniaxial compression curve defining the hardening function $b(\epsilon_p)$, Eq. (1), has been obtained, until peak, as the average of the three uniaxial compression curves rescaled to the same average peak coordinates: after peak the behavior is assumed perfectly plastic.

Fig. 9 shows the load/vertical displacement (F/u) curves obtained with the three discretizations of Fig. 8 when the critical index of local stiffness release is equal to the tensile strength of the material ($\alpha = 1$). The initial elastic slope of the F/u curves captured by the bimodulus approach is in good agreement with the experimental results. The analyses converged smoothly and the qualitative features of the response were reproduced; smeared fracture localized in the column of elements right above the sharp-edged notch. The three runs did not show significant mesh sensitivity. However, quantitative prediction is far from being reached: the bearing capacity and the amount of energy dissipation are considerably underestimated.

Due to this observation, and also considering that the value of tensile strength is quite uncertain, we performed a parametric study on parameter α, Eq. (11). Fig. 10 shows the results for the coarse mesh and for the three values of $\alpha = 1, 1.5, 2$. It is shown that $\alpha = 1.5$ still underestimates peak load but captures well the softening tail; whereas for $\alpha = 2$, a good estimate of bearing capacity is obtained but with excess of energy dissipation. This shows the intrinsic limits of the present smeared crack approach to brittle fracture of notched specimens. However, the procedure of stiffness release was performed

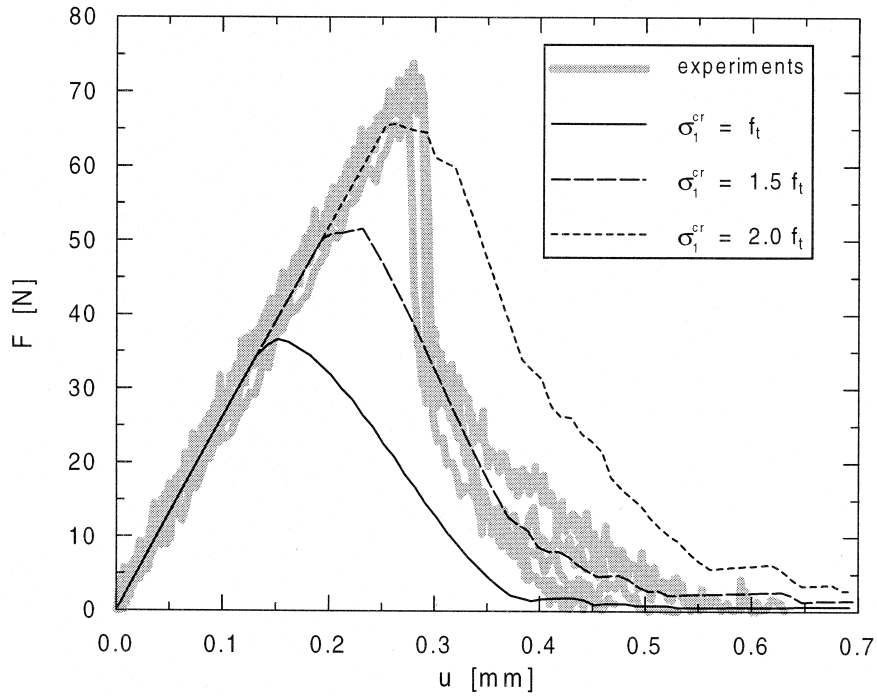

Fig. 10. Load/displacement curves of syntactic foam Tencara 2000™ TPB test: Modified Drucker–Prager model with use of stiffness release technique based on critical value of the maximum principal stress σ_1; parametric study of different threshold values σ_1^{cr} (coarse mesh).

successfully in the computer simulations of the composite sandwich panels under three and four point bendings (Corigliano et al., 1999).

Alternative to the present smeared crack approach, other models proposed in the literature could also be employed. For the sake of comparison, we also tested two other models available in the computer code. Both are based on classical multisurface plasticity (Willam et al., 1986; Feenstra and de Borst, 1996) and smeared crack concepts (Rots and Blaauwendraad, 1989; Guzina et al., 1995); the second is implemented in an explicit integration environment. While runs with the first model encountered problems of convergence for the finer meshes, even if an indirect load/displacement control (Riks, 1979) was used, the second model, similar in principle to the approach followed here, provided a good quantitative and mesh-insensitive estimate of the F/u curve when the fracture-energy-based regularization approach was used (Willam et al., 1986).

5.2.2. Discrete crack approach

Fig. 11 gives the load/vertical displacement curve for the case of the classical linear cohesive law identified in Section 4.2.1. As expected for the discrete approach, under mesh refinement the results are practically mesh-objective. The softening tail is captured well, whereas peak load is underestimated but with conspicuous improvement with respect to the smeared approach. Then, a parametric study has been conceived on the trapezoidal cohesive crack law based on parameter β. Fig. 12 reports the best quantitative simulations of the TPB test: the Dugdale-type law ($\beta = 1$) renders the highest peak prediction and brittler, almost vertical, initial post-peak branch. Other analyses based on a dual trapezoidal cohesive law with horizontal plateau at constant σ_{n_u} also gave interesting results and similar

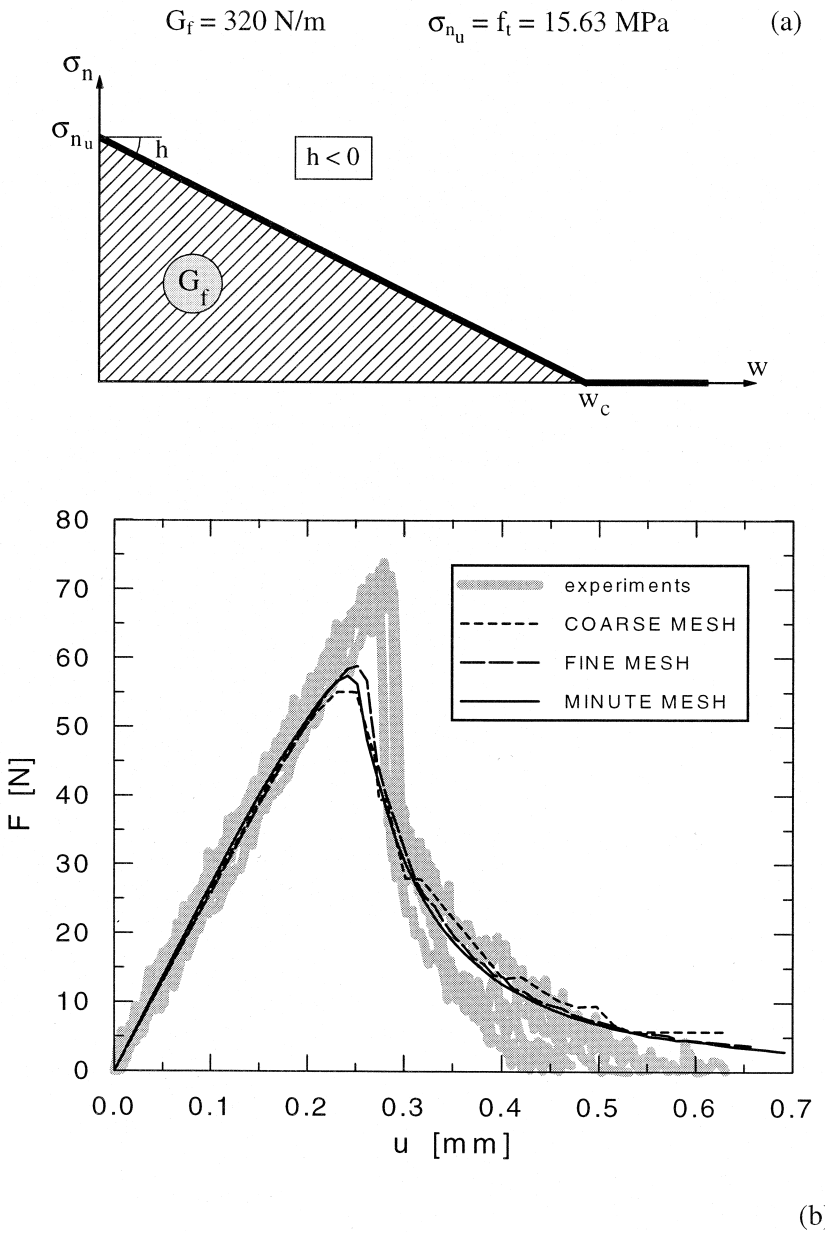

Fig. 11. Load/displacement curves of syntactic foam Tencara 2000™ TPB test: elastic bulk material with linear cohesive law on mid-span ligament section; (a) linear cohesive law and material parameters, (b) experimental and numerical responses.

trends, but some problems of convergence were encountered for some of the curves giving rise to initial snap-back branches.

In conclusion, it seems that the hypothesis of a material that is able to substain constant stress until a critical opening displacement is reached, and then fails abruptly, seems to be the nearest to phenomenological reality for the foam under study. This appears to be connected with the underlying

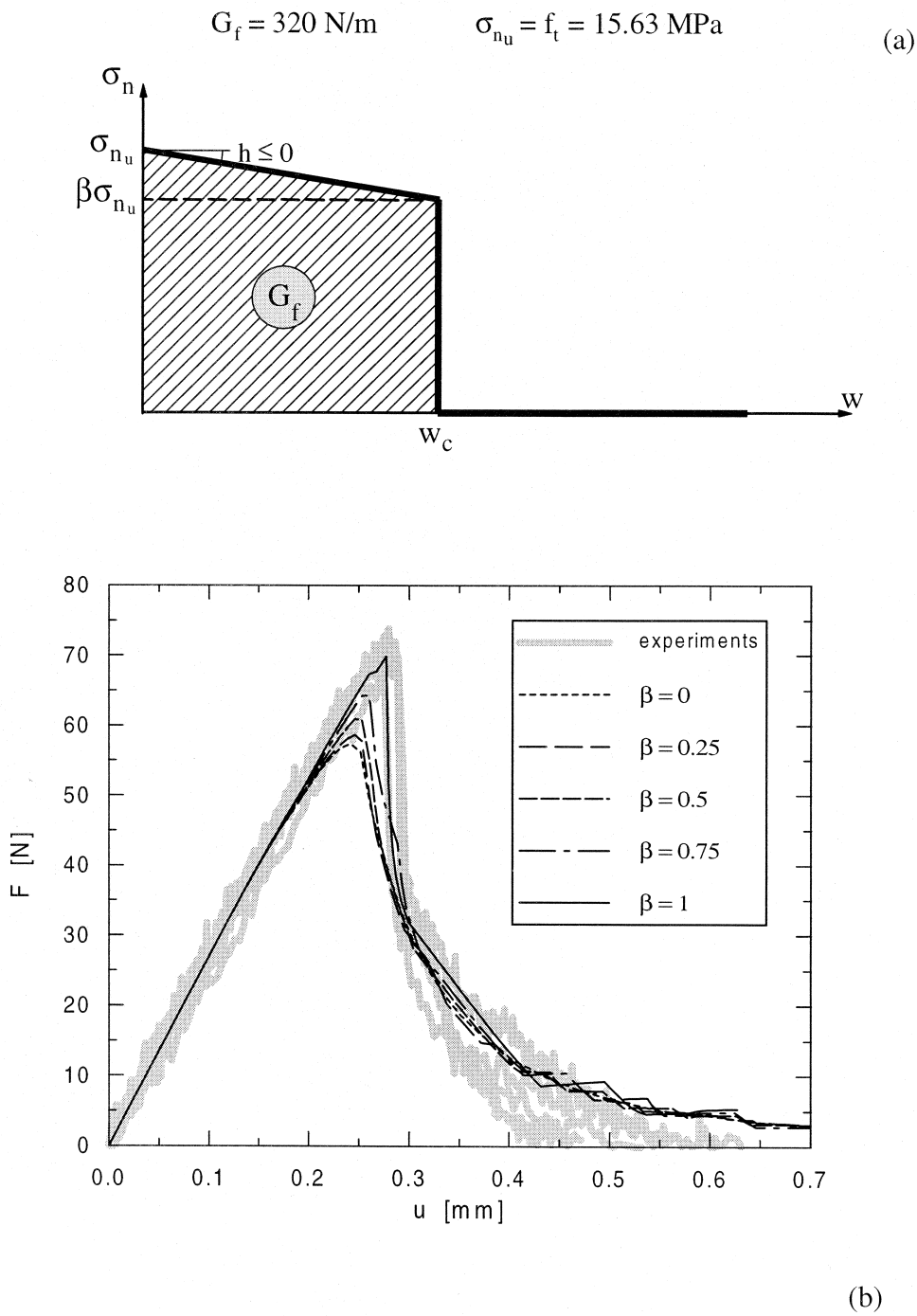

Fig. 12. Load/displacement curves of syntactic foam Tencara 2000™ TPB test: elastic bulk material with trapezoidal cohesive law on mid-span ligament section. Parametric study on parameter β (minute mesh): (a) trapezoidal cohesive law and material parameters, (b) experimental and numerical responses.

structure of a polymeric material, where the long molecular chains first need to be reoriented before rupturing (Knauss, 1973). As reported by Schapery (1975) and Kanninen and Popelar (1985), cohesive fracture laws of Dugdale-type have been previously used for modeling time-independent and time-dependent fracture processes in polymeric materials (Kostrov and Nikitin, 1970).

6. Conclusions

The paper presented the main results of an experimental campaign and a numerical investigation on the mechanical behavior of a syntactic foam used as light core material for composite sandwich panels. Uniaxial tension/compression, biaxial compression and TPB tests were investigated. The observed features allowed to locate proper constitutive models for the mechanical behavior at the macroscopic scale. A bimodulus Modified Drucker–Prager model has been calibrated on the basis of the biaxial tests. A cohesive crack approach has been implemented to capture the fracture process of the TPB test. Different two- and three-parameter cohesive laws have been tested: the rectangular Dugdale-type cohesive law with tensile strength and Mode-I fracture energy calibrated from uniaxial tension and TPB tests showed the best performance and allowed full quantitative agreement with the experimental findings.

The engineering mechanics approach followed here does not propose particularly innovative experimental or computational procedures. However, due to the scarcity of comprehensive investigations on the mechanical behavior of syntactic foams, the authors' personal belief is that the results presented here should contribute to this specific branch of composite mechanics. The present study is purely phenomenological (a micromechanical homogenization approach to model the elastic behavior of the same syntactic foam has been proposed by Bardella and Genna, 1999) and represents only a preliminary investigation: there is a wide open ground for further developments along different directions in both experimental and numerical aspects, including, for instance, mixed-mode fracture, unnotched specimen testing, enquiry of strain localization phenomena, triaxial and fatigue behaviors, rate and temperature dependencies.

Acknowledgements

The present paper originated from a research project between Intermarine SpA and Politecnico di Milano headed by Prof. Giulio Maier at the Department of Structural Engineering. At that time, author Egidio Rizzi was an employee of Politecnico di Milano. The authors wish to thank Intermarine SpA for providing reference material on composites for naval engineering applications and for granting permission to publish the present results. We are grateful to Prof. Giulio Maier for involving us into this research topic and for fruitful discussions on selected related subjects. We acknowledge the contributions of our former students Ivan Baroncioni, Paolo Ferrari and Luca Lobaccaro who were involved in the present research during the preparation of their Laurea theses.

References

Alvaredo, A.M., Torrent, R.J., 1987. The effect of the shape of the strain-softening diagram on the bearing capacity of concrete beams. Materials and Structures 20, 448–454.

Bard, Y., 1974. Nonlinear Parameter Estimation. Academic Press, New York.

Bardella, L., Genna, F., 1999. Effective elastic moduli of syntactic foams, I. J. Solids and Structures. submitted.

Barenblatt, G.I., 1962. Mathematical theory of equilibrium cracks in brittle fracture. Advances in Applied Mechanics 7, 55–129.
Bažant, Z.P., 1996. Analysis of work-of-fracture method for measuring fracture energy of concrete. J. of Engineering Mechanics, ASCE 122 (2), 138–144.
Cen, Z., Maier, G., 1992. Bifurcations and instabilities in fracture of cohesive-softening structures: a boundary element analysis. Fatigue and Fracture of Engineering Materials and Structures 15 (9), 911–928.
Corigliano, A., Rizzi, E., Papa, E., 1999. Experimental characterization and numerical simulations of a syntactic foam/glass fibre composite sandwich, Composite and Technology. Submitted.
Cornelissen, H.A.W., Hordijk, D.A., Reinhardt, H.W., 1986. Experimental determination of crack softening characteristics of normalweight and lightweight concrete. HERON 31 (2), 45–56.
Curnier, A., He, Q.-C., Zysset, P., 1995. Conewise linear elastic materials. J. of Elasticity 37, 1–38.
DeRuntz, J.A., Hoffman, O., 1969. The static strength of syntactic foams. J. of Applied Mechanics, Transactions of the ASME 36 (E3), 551–557.
DeRuntz, J.A., 1971. Some applications of plasticity theory to statics of syntactic foam. J. of Applied Mechanics, Transactions of the ASME 38 (E4), 23–29.
Dugdale, D.S., 1960. Yielding of steel sheets containing slits. J. of the Mechanics and Physics of Solids 8, 100–104.
Feenstra, P.H., de Borst, R., 1996. A composite plasticity model for concrete. Int. J. of Solids and Structures 33 (5), 707–730.
Guinea, G.V., Elices, M., Planas, J., 1997. On the initial shape of the softening function of cohesive materials. Int. J. of Fracture 87, 139–149.
Guzina, B.B., Rizzi, E., Willam, K., Pak, R.Y.S., 1995. Failure prediction of smeared-crack formulations. J. of Engineering Mechanics, ASCE 121 (1), 150–161.
Hibbitt, H.D., Karlsson, B., Sorensen, P., 1998. ABAQUS Manuals, ver. 5.8, Hibbitt. Karlsson and Sorensen Inc, Pawtucket, RI, USA.
Hiel, C., Dittman, D., Ishai, O., 1993. Composite sandwich construction with syntactic foam core. A practical assessment of post-impact damage and residual strength. Composites 24 (5), 447–450.
Hillerborg, A., Modeer, M., Petersson, P.E., 1976. Analysis of crack formation and crack growth in concrete by means of fracture mechanics and finite elements. Cement and Concrete Research 6, 773–782.
Hollaway, L., 1990. Polymer, fibre and composite material properties and manufacturing techniques. In: Hollaway, L. (Ed.), Polymers and Polymers Composites in Construction. Thomas/Telford, London, pp. 5–31.
Hull, D., Clyne, T.W., 1996. An Introduction to Composite Materials. Cambridge University Press, Cambridge.
Kanninen, M.F., Popelar, C.H., 1985. Advanced Fracture Mechanics. Oxford University Press, New York.
Karihaloo, B.L., 1995. Fracture Mechanics and Structural Concrete. Longman Scientific & Technical, Harlow, UK.
Kenyon, A.S., 1968. Role of the interface in glass–epoxy composites. J. of Colloid and Interface Science 27 (4), 761–771.
Knauss, W.G., 1973. The mechanics of polymer fracture. Applied Mechanics Reviews 26 (1), 1–17.
Kostrov, B.V., Nikitin, L.V., 1970. Some general problems of mechanics of brittle fracture. Archiwum Mechaniki Stosowanej 6 (22), 749–776.
Lee, H., Neville, K., 1973. Epoxy-resin foams. In: Frisch, K.C., Saunders, J.H. (Eds.), Plastic Foams. Marcel Dekker, New York, pp. 701–733.
Luxmoore, A.R., Owen, D.R.J., 1982. Syntactic foams. In: Hilyard, N.C. (Ed.), Mechanics of Cellular Plastics. Applied Science Publishers, London, pp. 359–391.
Maier, G., Novati, G., Cen, Z., 1993. Symmetric Galerkin boundary element method for quasi-brittle fracture and frictional contact problems. Computational Mechanics 13, 74–89.
Mildner, R.C., Nacke, K.F., Veazey, E.W., Woodland, P.C., 1970. Blocking multi-pair cable with plastic-microsphere syntactic foam. Modern Plastics 47 (5), 98–99.
Narkis, M., Puterman, M., Kenig, S., 1980. Syntactic foam. Part II: Preparation and characterization of three-phase systems. J. of Cellular Plastics 16, 326–330.
Nicolais, L., Nicodemo, L., 1973. Strength of particulate composite. Polymer Engineering and Science 13 (6), 469.
Nielsen, L.E., 1983. Elastic modulus of syntactic foams. J. of Polymer Science: Polymer Physics Edition 22, 1567–1568.
Okuno, K., Woodhams, R.T., 1974. Mechanical properties and characterization of phenolic resin syntactic foams. J. of Cellular Plastics 10, 237–244.
Palchak, R.J.F., 1973. Military and space applications of cellular materials. In: Frisch, K.C., Saunders, J.H. (Eds.), Plastic Foams. Marcel Dekker, New York, pp. 955–983.
Palumbo, M., Donzella, G., Tempesti, E., Ferruti, P., 1996. On the compressive elasticity of epoxy resins filled with hollow glass microspheres. J. of Applied Polymer Science 60, 47–53.
Papa, E., Corigliano, A., Rizzi, E., 1999. Mechanical behavior of a syntactic foam/glass fibre composite sandwich: experimental results, Composite Structures. Submitted.
Parodi, F., 1989. Materiali compositi a matrice termoindurente (in Italian). In: Proc. Scuola su Materiali Polimerici, Gargnano (BS), 11–16 June. AIM, Tecnoprint, Bologna, Italy, 165–227.

Puterman, M., Narkis, M., Kenig, S., 1980. Syntactic foam. Part I: Preparation, structure and properties. J. of Cellular Plastics 16, 223–229.

Riks, E., 1979. An incremental approach to the solution of snapping and buckling problems. Int. J. of Solids Structures 15, 529–551.

RILEM, 1985. Determination of the fracture energy of mortar and concrete by means of three-point bend tests on notched beams. RILEM Recommendation. Materials and Structures, Paris, France 18 (106), 285–290.

Rots, J.G., Blaauwendraad, J., 1989. Crack models for concrete: discrete or smeared? Fixed, multi-directional or rotating? HERON 34 (1).

Sahu, S., Broutman, L.J., 1972. Mechanical properties of particulate composites. Polymer Engineering and Science 12 (2), 91–100.

Scarponi, C., Briotti, G., Barboni, R., Marcone, A., Iannone, M., 1996. Impact testing on composite laminates and sandwich panels. J. of Composite Materials 30 (17), 1873–1911.

Schapery, R.A., 1975. A theory of crack initiation and growth in viscoelastic media. Part I: Theoretical development. Int. J. of Fracture 11 (1), 141–159.

Shutov, F.A., 1986. Syntactic polymer foams. Advances in Polymer Science 73/74, 63–123.

Smith, C.S., 1990. Design of Marine Structures in Composite Materials. Elsevier Applied Science, London.

Sternfield, A., 1982. New types and sources of micro-spheres can help widen RP markets. Modern Plastics International 12 (6), 43–45.

Thomas, C.R., 1973. Syntactic carbon foams. Materials Science and Engineering 12, 219–233.

Wei, D., Baptiste, D., Bompard, Ph., François, D., 1989. A damage micromechanics approach to heterogeneous material. In: Mazars, J., Bažant, Z.P. (Eds.), Cracking and Damage, Strain Localization and Size Effect. Elsevier, New York, pp. 128–139.

Willam, K., Bićanić, N., Pramono, E., Sture, S., 1986. Composite fracture model for strain softening computations of concrete. In: Wittmann, F.H. (Ed.), Proc. Symp. Fracture Toughness and Fracture Energy of Concrete. Elsevier, Amsterdam, pp. 149–162.